Modulation of long-range neural synchrony reflects temporal limitations of visual attention in humans

Joachim Gross*, Frank Schmitz*, Irmtraud Schnitzler*, Klaus Kessler*, Kimron Shapiro†, Bernhard Hommel‡, and Alfons Schnitzler*§

*Department of Neurology, Heinrich-Heine University, 40225 Düsseldorf, Germany; †University of Wales, Bangor LL57 2DG, Wales; and ‡Leiden University, 2300 RA, Leiden, The Netherlands

Communicated by Anne Treisman, Princeton University, Princeton, NJ, July 27, 2004 (received for review March 14, 2004)

Because of attentional limitations, the human visual system can process for awareness and response only a fraction of the input received. Lesion and functional imaging studies have identified frontal, temporal, and parietal areas as playing a major role in the attentional control of visual processing, but very little is known about how these areas interact to form a dynamic attentional network. We hypothesized that the network communicates by means of neural phase synchronization, and we used magnetoencephalography to study transient long-range interarea phase coupling in a well studied attentionally taxing dual-target task (attentional blink). Our results reveal that communication within the fronto-parieto-temporal attentional network proceeds via transient long-range phase synchronization in the beta band. Changes in synchronization reflect changes in the attentional demands of the task and are directly related to behavioral performance. Thus, we show how attentional limitations arise from the way in which the subsystems of the attentional network interact.

The human brain faces an inestimable task of reducing a potentially overloading amount of input into a manageable flow of information that reflects both the current needs of the organism and the external demands placed on it. This task is accomplished via a ubiquitous construct known as "attention," whose mechanism, although well characterized behaviorally, is far from understood at the neurophysiological level. Whereas attempts to identify particular neural structures involved in the operation of attention have met with considerable success (1–5) and have resulted in the identification of frontal, parietal, and temporal regions, far less is known about the *interaction* among these structures in a way that can account for the task-dependent successes and failures of attention. The goal of the present research was, thus, to unravel the means by which the subsystems making up the human attentional network communicate and to relate the temporal dynamics of their communication to observed attentional limitations in humans.

A prime candidate for communication among distributed systems in the human brain is neural synchronization (for review, see ref. 6). Indeed, a number of studies provide converging evidence that long-range interarea communication is related to synchronized oscillatory activity (refs. 7–14; for review, see ref. 15). To determine whether neural synchronization plays a role in attentional control, we placed humans in an attentionally demanding task and used magnetoencephalography (MEG) to track interarea communication by means of neural synchronization.

In particular, we presented 10 healthy subjects with two visual target letters embedded in streams of 13 distractor letters, appearing at a rate of seven per second. The targets were separated in time by a single distractor. This condition leads to the "attentional blink" (AB), a well studied dual-task phenomenon showing the reduced ability to report the second of two targets when an interval <500 ms separates them (16–18). Importantly, the AB does not prevent perceptual processing of missed target stimuli but only their conscious report (19), demonstrating the attentional nature of this effect and making it a good candidate for the purpose of our investigation.

Although numerous studies have investigated factors, e.g., stimulus and timing parameters, that manipulate the magnitude of a particular AB outcome, few have sought to characterize the neural state under which "standard" AB parameters produce an inability to report the second target on some trials but not others. We hypothesized that the different *attentional states* leading to different behavioral outcomes (second target reported correctly or not) are characterized by specific patterns of transient long-range synchronization between brain areas involved in target processing.

Showing the hypothesized correspondence between states of neural synchronization and human behavior in an attentional task entails two demonstrations. First, it needs to be demonstrated that cortical areas that are suspected to be involved in visual-attention tasks, and the AB in particular, interact by means of neural synchronization. This demonstration is particularly important because previous brain-imaging studies (e.g., ref. 5) only showed that the respective areas are active within a rather large time window in the same task and not that they are concurrently active and actually create an interactive network. Second, it needs to be demonstrated that the pattern of neural synchronization is sensitive to the behavioral outcome; specifically, the ability to correctly identify the second of two rapidly succeeding visual targets.

Materials and Methods

Subjects, Paradigm, and Recording. Recordings were obtained from 10 healthy, right-handed subjects with the local ethics committee's approval. All subjects gave their informed consent. Each experimental trial consisted of 15 capital white letters that were visually presented as a rapid serial visual presentation (RSVP) stream on a back-projection screen. Each letter was presented with a visual angle of 3.72° at a distance of 1.2 m. Stimulus duration was 44 ms and the interstimulus interval was 102 ms, yielding a stimulus onset asynchrony (SOA) of 146 ms. Presented were 27–30 blocks, each containing 72 trials. Each block consisted of 24 trials with no targets, 24 trials with one target, 12 trials with two targets separated by one distractor (SOA of 292 ms), and 12 trials with two targets separated by five distractors (SOA of 876 ms). The first target could appear at position 4, 5, or 6 in the letter stream. For five subjects, "X" and "O" were used as targets, and for the other five subjects "L" and "T" were used as targets.

After each stream presentation, subjects were asked to report all targets in the correct order. The analysis was based on the following conditions: detected single-target trials ("target"), trials with no targets ("distractor"), and trials with two targets separated by one distractor where either both were detected

Abbreviations: AB, attentional blink; ROI, region of interest; SI, phase synchronization index; TFR, time–frequency representation.

§To whom correspondence should be addressed at: Department of Neurology, MEG, Heinrich-Heine University, Moorenstrasse 5, 40225 Duesseldorf, Germany. E-mail: schnitza@uni-duesseldorf.de.

www.pnas.org/cgi/doi/10.1073/pnas.0404944101

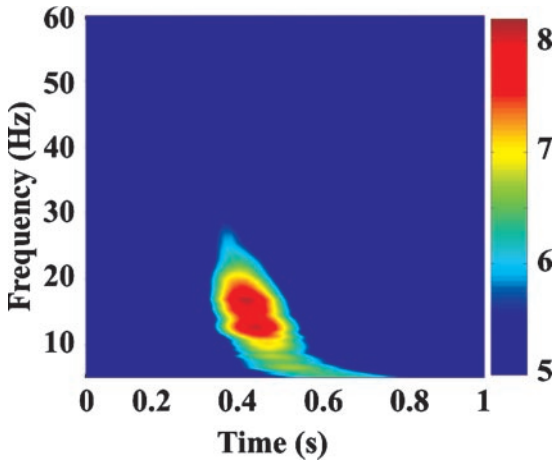

Fig. 1. TFR for the distractor condition subtracted from the target condition. Time 0 marks the onset of the target. The TFR represents the average across subjects and channels and is displayed in units of standard deviation of the baseline (thresholded at a value of 5). TFRs have been normalized for each frequency before averaging.

correctly (no-AB) or where the second target was not detected (AB). We complied with the results of several studies that have demonstrated that the presence of stimuli after each target (termed "masks") is a necessary condition for the occurrence of the AB effect (20, 21).

Neural activity was recorded with a Neuromag (Helsinki) 122 whole-scalp neuromagnetometer (22) in a magnetically shielded room. MEG signals were recorded with a passband of 0.03–175 Hz and digitized with 514 Hz. High-resolution T1-weighted magnetic resonance images were obtained for each subject.

Analysis. To localize the areas involved in the processing of targets, we determined a time–frequency signature of target processing. To this end, time–frequency representations (TFRs) were calculated, averaged over all sensors, and time-locked to the presentation of all correctly reported targets. TFRs were computed on single trials (down-sampled by a factor of 4) in the frequency range of 5–60 Hz at 50 geometrically sampled frequencies by using morlet wavelets. The TFRs were normalized for each frequency by subtracting the mean baseline value and dividing by the baseline standard deviation (7). The baseline was defined as the 200 ms preceding the onset of the first letter.

The same computation was performed for trials containing only distractor letters matched with the stream positions where targets could occur. Distractor TFRs were subtracted from the corresponding target TFRs to reveal the time and frequency window showing strongest reactivity to target presentation. The subtraction eliminates components common to target and distractor processing. Strongest target-related activity was seen in the beta band (13–18 Hz) at a time of about 400 ms after target onset (Fig. 1). Subsequent analysis was focused on the wavelet transform centered at 15 Hz by using a morlet wavelet (width of 6 Hz). The wavelet transform was used to compute the cross-spectral density of all combinations of channels in the chosen time–frequency area, allowing the dynamic imaging of coherent sources (DICS) (23) localization for all 10 subjects. DICS uses spatial filters in the frequency domain to create tomographic functional maps based on power that are displayed on the individual anatomic MR images. The individual functional maps represent the spatial distribution of 15-Hz power at a latency of 400 ms (with a voxel size of 6 mm) in the entire brain.

The individual power maps were spatially normalized and smoothed (12 mm) by using SPM99. The normalized maps were subjected to a permutation analysis in SnPM99 (SPM99, SnPM99, Wellcome Department of Cognitive Neurology, Institute of Neurology, London) that resulted in the identification of eight significant regions of interest (ROIs): occipital, cingulum, frontal left and right, temporal left and right, and posterior parietal left and right. Segmentation of the network was based on local maxima in the group statistics map. For each ROI, the 10 sensors being most sensitive to the region were selected and used for the subsequent analysis.[¶]

Synchronization analysis based on the wavelet transforms was performed for all four conditions and for nine subjects (one subject had to be excluded because of artifacts). The phase synchronization index (SI) quantifies the phase coupling between different regions. It is computed as the absolute value of the sum of the complex phase differences of both regions divided by the number of epochs and is bounded between 0 (indicating no phase locking) and 1 (indicating perfect phase locking). Visual inspection of the time courses of SI in the no-AB condition for all connections revealed either a modulation at the rate of stimulation (7 Hz) or two maxima separated by about 292 ms (the delay between the two targets in this analysis). Based on this observation, connections were classified as stimulus-related (type A connection, Fig. 3*B Left*) or target-related (type B connection, Fig. 3*B Right*) by using the autocorrelation of each SI time course. Stimulus-related connections are characterized by similar components in the SI time course that appear at the rate of stimulus presentation. This stimulus relatedness leads to a peak in the autocorrelation at a lag of about 146 ms. In contrast, the SI of target-related connections is dominated by peaks separated by about 292 ms, leading to a peak in the autocorrelation at a lag of about 292 ms (the delay between both targets). For significance testing, the autocorrelation of 1,000 random permutations of each SI time course was computed, and the 99th percentile for each lag (dashed line in Fig. 3*B*) was compared with the original autocorrelation (solid line in Fig. 3*B*).

In addition to a significant autocorrelation at lag 146 (type A connections) or at lag 292 (type B connections), SI after stimulation onset had to rise above the 95th percentile of the prestimulus baseline for the AB and the no-AB condition to be subjected to further analysis. To eliminate the possibility that modulation of SI is solely due to power changes, we repeated the SI computation with random changes of phase for each trial[‖] and rejected connections that showed SI values below the 95th percentile of this surrogate data.

Significance testing of SI differences was performed by using the Kruskal–Wallis test. Differences that are described as significant have a $P < 0.05$ and were corrected for multiple tests (Bonferroni).

Results

Subjects showed an overall high performance in the single-target (baseline) condition (87.6% on average) and to the first target in dual-target conditions (87.8% for short lag and 91.0% for long lag) that did not depend on the target position in the letter stream. As expected from the literature, the AB effect was evident in the dual-target condition as a decrease in performance for the short lag (292 ms). On average, only 61.3% of the second targets were identified correctly, whereas performance returned to the single-target baseline (90.2%) by the long lag (876 ms). Fig. 1 shows the difference TFR between targets and distractors. The beta-frequency range (≈15 Hz) shows an en-

[¶]Although the synchronization analysis is necessarily more sensitive to adjacent regions of cortex as per the eight identified ROIs, the highest degree of synchronization as reported subsequently is found for highly separate cortical areas.

[‖]For each trial and channel group, phases were randomly shifted, thereby destroying phase synchronization.

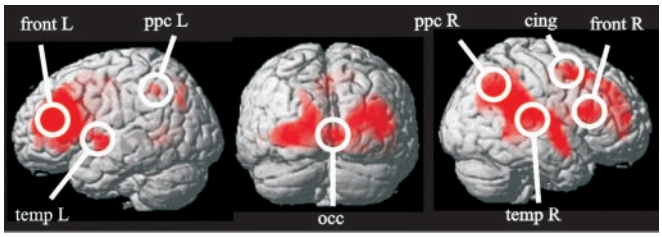

Fig. 2. Localization of the time–frequency target component displayed in Fig. 1. Functional maps of oscillatory power in the beta band were computed for each subject. The functional maps were spatially normalized by using SPM99, and a permutation analysis with SnPM99 was performed. Only areas with a significance of $P < 0.01$ (corrected) are shown. The maximum of each ROI is marked and labeled and was used for further computations. A single occipital ROI was used.

hancement at a latency of about 400 ms after stimulus presentation (Fig. 1). The enhancement represents a phenomenon that distinguishes target from distractor processing and was used to localize brain areas involved in target processing.

Statistical permutation analysis of localization across the group resulted in the identification of eight significant ROIs across subjects (Fig. 2 and Table 1): occipital (occ), frontal left (frontL), frontal right (frontR), temporal left (tempL), temporal right (tempR), posterior parietal left (ppcL), posterior parietal right (ppcR), and cingulum (cing).

The phase synchronization of the 28 possible connections showed different responses to targets and distractors. For some connections, the SI was modulated by each stimulus similarly (regardless of the stimulus being a distractor or target), and for others, the SI was modulated mainly by targets (showing little effect for distractors). Consequently, connections were classified as type A (stimulus-related, i.e., each stimulus leads to a modulation of the SI) or type B (target-related, i.e., mainly targets modulate the SI) connections (see *Materials and Methods*) by using the no-AB condition, because in this condition two targets were presented (separated by 292 ms) and reported correctly.**

Fig. 3*A Left* shows an example of a typical stimulus-related connection. Peaks in the SI are separated by about 146 ms, corresponding to the rate of stimulus presentation. No specific effect of the targets (which are presented at 0 ms and 292 ms) can be observed, indicating similar processing of all stimuli. Consequently, the autocorrelation of the SI time course reveals a peak at a lag of about 146 ms (Fig. 3*B Left*).

**Only connections that passed the significance tests described in *Materials and Methods* were classified.

Table 1. Talairach–Montreal Neurological Institute (Talairach-MNI) coordinates of areas obtained from the localization of the target component

Area	Talairach-MNI coordinates
Occipital	(−10,−52,0), (16,−52,4)
Posterior parietal right	(52,−54,40), (30,−70,44)
Posterior parietal left	(−26,−74,46)
Temporal right	(38,−10,−4)
Temporal left	(−42,−6,−6)
Frontal right	(46,22,20)
Frontal left	(−44,32,24), (−44,36,−6), and (−20,50,24)
Cingulum	(6,0,46), (−4,−10,42)

Significant local maxima ($P < 0.01$, corrected) were extracted and resulted in eight cortical ROIs. Mean coordinates were used in case of multiple local maxima in a region and are displayed in Fig. 2.

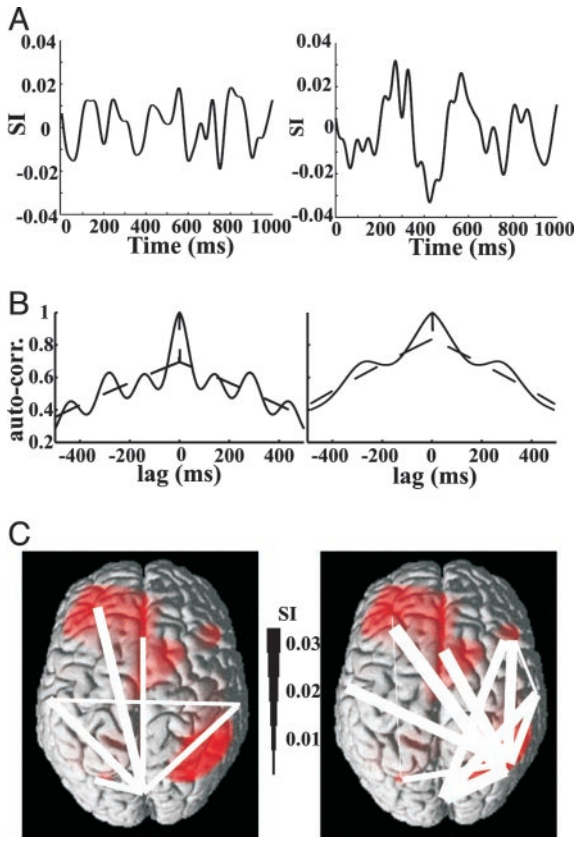

Fig. 3. Classification of stimulus- and target-related connections. (*A*) SI for one subject for a typical stimulus-related (*Left*, occipital to posterior parietal left) and a typical target-related (*Right*, frontal left to posterior parietal right) connection. SI was computed based on sensor groups that are most sensitive to a given region. (*B*) Autocorrelations were computed for the time course of synchronization for each pair of connections. Connections showing a significant peak at 146 ms were classified as stimulus-related (*Left* shows an example, to cingulum), and connections showing a significant peak at 292 ms were classified as target-related (see *Right* for an example, frontal left to frontal right). The dashed line represents the 99% confidence limit computed from 1,000 random permutations of the SI time course. (*C*) The stimulus-related (*Left*) and target-related (*Right*) networks are shown with linewidth coding for the strength of synchronization at 260 ms.

In contrast, the synchronization of a target-related connection (Fig. 3*A Right*) is dominated by two peaks separated by about 292 ms (the temporal separation of the two presented targets), reflecting target processing. The two peaks in the SI lead to a peak at a lag of ≈292 ms in the autocorrelation (Fig. 3*B Right*).

Type A connections primarily link the occipital cortex to left hemisphere areas (Fig. 3*C Left*). In contrast, type B connections show a remarkably different pattern. Here, the strongest connections are observed between right posterior parietal and cingulum and left temporal and frontal regions (Fig. 3*C Right*).

To take advantage of our ability to relate underlying neurophysiology to behavior and to show that successful attentional selection mirrors the changing state of this network, we analyzed the temporal dynamics of trials when dual-target interference prevented the second target from being reported (AB) as compared with trials when it could be reported (no-AB). This analysis revealed two significant effects.

First, in the no-AB condition, the phase synchronization during the entire stream is significantly enhanced compared with the AB condition. Fig. 4*A* shows the temporal evolution of the SI in the no-AB (solid line) and AB (dashed line) conditions. Zero corresponds to the onset of the first target. The stream

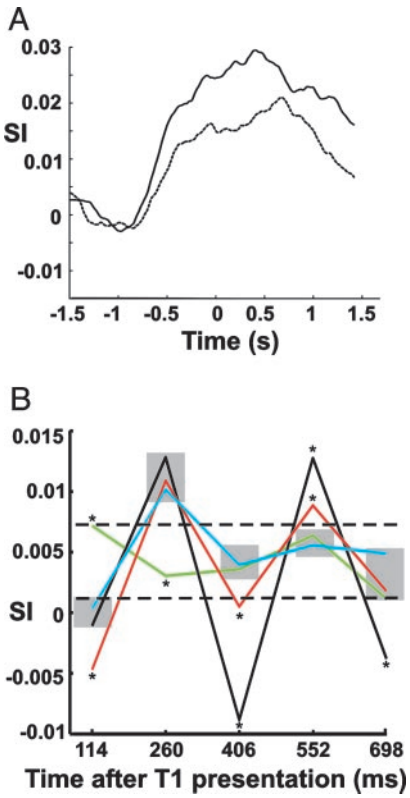

Fig. 4. Mean synchronization (SI) in the target-related network. (*A*) The no-AB condition (solid line) shows a stronger SI during stimulus presentation than that in the AB condition (dashed line). Zero milliseconds corresponds to the onset of the first target. The beginning of the letter stream ranges from −880 to −580 ms. The SI time courses were smoothed with a Savitzky–Golay filter (polynomial order, 3; frame length, 600) and averaged across all significant connections within the target-related network. (*B*) SI for the components of five successive stimuli. The *x* axis specifies time after presentation of the first target. Each point represents the mean SI in a 60-ms window centered at 260 ms after the respective stimulus. Values at 260 ms quantify the network synchronization to the first target, and values at 114 ms represent the network synchronization corresponding to the distractor preceding the first target. Conditions are color-coded (black, no-AB; red, AB; blue, target; green, distractor). The dashed lines mark the extent of SI in trials containing only distractors. Points marked with an asterisk are significantly different from their neighbors at the same position ($P < 0.05$, Kruskall–Wallis test), whereas points within the same shaded area are not significantly different. Negative values arise from the filtering of the SI time courses.

onset is between −880 ms and −580 ms (depending on the target position in the stream). The significantly stronger increase of the SI in the target-related network for the no-AB condition (solid line) than in the AB condition (dashed line) can clearly be seen.

Second, the temporal *modulation* of synchronization by targets and masks is significantly stronger in the no-AB condition than in the AB condition.

To study this second effect, i.e., SI modulation, the global phase synchronization increase was removed by applying a 2- to 20-Hz bandpass filter to the SI time courses. The filter removes the slow changes in the SI time course (Fig. 4*A*) while preserving the modulation. The strongest target-related modulation of the SI was evident at 260 ms after target presentation and is termed the "network response component." This synchronization component was used to summarize the response of the target-related network to the different stimuli in the different conditions (Fig. 4*B*).

The *x* axis in Fig. 4*B* specifies time after presentation of the first target (T1). Each point represents the mean SI in a 60-ms window centered at 260 ms after a stimulus occurred.[††] Thus, the mean SI values at 114 ms represent the "network response component" to the distractor preceding the first target, and the values at 260 ms represent the network response to the first target. It should be noted that the network response 260 ms after a stimulus is also affected by the following stimulus (which follows the preceding stimulus after 146 ms). This is evident in Fig. 4*B*. All conditions with a target show a reduced response component to the distractor preceding the target than that in trials containing only distractors (green line). This desynchronization likely represents an active suppression of irrelevant stimuli to prepare and protect target processing. Thus, the desynchronization likely marks the transition between different processing states (7). We speculate that desynchronization before a target may represent an active suppression of distractor processing, freeing the system resources for target processing, as well as protecting the target against interference. The network response component to the first target (black, red, and blue lines at 260 ms) is stronger than that in the distractor condition (green line), likely reflecting the preferred identification and preferred processing of behaviorally relevant stimuli. In the no-AB condition (black line) the distractor following the first target elicits a reduced network response (desynchronization at 406 ms), followed by a strong synchronization to the second target (552 ms). Again, the desynchronization at 406 ms may signify the suppression of the distractor, whereas the successful processing of the second target (both targets were correctly reported in this condition) is associated with a strong synchronization (at 552 ms).

Interestingly, the trials in which the second target was not reported (AB condition) show a different pattern (red line). First, the desynchronization to the distractor after T1 is significantly smaller, and, second, the synchronization to T2 is significantly smaller than that in the no-AB condition. Thus, it seems that, in the AB condition, the decreased selectivity of the system enables the second mask to make additional (undesirable) demands on processing capacity and may actually substitute the neural representation of the second target, as has been shown behaviorally (21, 24).

By looking at the modulation of the individual connections (Table 2), we can further identify the connections that show the strongest differences between conditions. The task effect is evident as stronger synchronization (to second target) and desynchronization (to mask) in the no-AB condition than in the AB condition. Thus, modulation was quantified as difference of synchronization and desynchronization for both conditions. The difference between conditions (Table 2) is strongest for the connections that show the largest task effect, namely, frontL–ppcR, ppcR–cing, ppcL–ppcR, and occ–ppcR.

Discussion

The aim of this study was to identify the correspondence between states of neural synchronization and human behavior in an attention-demanding task, the AB, that has been well characterized behaviorally. The present results support our hypothesis that characteristic spatiotemporal synchronization patterns are associated with different attentional states leading to different behavioral outcomes. Our results demonstrate that distinct spatiotemporal patterns of transient, long-range phase synchronization in a fronto-temporo-parietal network distinguish conditions under which physically identical target stimuli can be reported (no-AB) or not reported (AB). Two main differences between these two conditions are evident. First, beta synchronization in the target-related network is significantly stronger during the entire stream in the no-AB condition than in the AB condition; and second, beta synchronization is significantly stronger to targets, and significantly weaker to masks, in the

[††]Negative values arise from the bandpass filter applied to the SI time course.

NEUROSCIENCE

Table 2. SI of the individual connections of the target-related network (Fig. 3*C Right*) for the no-AB and the AB condition at times 406 and 552 ms

Connection	No-AB 406 ms	AB 406 ms	No-AB 552 ms	AB 552 ms	Modulation	Significance, *P*
occ–front R	0.000	0.003	0.006	−0.002	0.011	1.5e–10
occ–temp R	0.003	0.004	0.008	0.001	0.008	1.5e–10
occ–ppcR	−0.016	−0.009	0.023	0.017	0.013	2.7e–4
frontL–ppcL	0.003	0.010	−0.004	−0.001	0.004	1.5e–10
frontL–ppcR	−0.019	0.005	0.016	0.015	0.025	1.5e–10
frontR–tempR	−0.000	−0.002	−0.003	−0.003	−0.002	3.9e–9
frontR–ppcR	−0.014	−0.005	0.014	0.011	0.012	1.5e–10
tempL–ppcR	−0.015	−0.004	0.011	0.015	0.007	1.6e–3
tempR–ppcR	−0.007	−0.003	0.018	0.014	0.008	2.4e–7
ppcL–ppcR	−0.009	0.002	0.021	0.013	0.019	6.6e–5
ppcR–cing	−0.012	0.002	0.018	0.012	0.02	2.7e–9

The table lists the SI values for the two main conditions, AB and no-AB, for the individual connections of the target-related network. It describes the main effect of the AB for the individual connections by listing the SI values at times 406 and 552 ms corresponding to the synchronization to the mask (distractor after the first target) and the second target. Task-related modulation was computed as (col4-col2) − (col5-col3), where col *n* denotes the *n*th column of the table. The last column shows significances of modulation computed with a Kruskal–Wallis test.

no-AB condition than in the AB condition. It could well be that both effects point to the same conclusion: General enhancement of synchronization likely represents a state of increased sensitivity to behaviorally relevant stimuli (i.e., higher vigilance), similar to the baseline enhancement of neuronal firing during focused attention (25).

Apart from providing evidence for the hypothesis under investigation, our findings also have important implications with respect to the anatomical and functional characterization of, and to the communication within, the visual–attentional network. We discuss these implications in turn.

The Target-Related Network. The cortical areas forming what we have called the target-related type B network have been linked to visual attention (2–5) and working memory (26–28), and our findings corroborate those of previous studies pointing to the same lateralization (right posterior parietal and left frontal). According to Desimone and Duncan (1), such a network may exert attentional control by biasing the processing of incoming visual information: Neural representations of target- or goal-related stimuli receive top-down (i.e., frontal) support, which increases their chances to win the competition for selection and, hence, their impact on overt behavior. Specifically, the components of our target-related (B) network likely represent the neural components responsible for coding the task-related stimuli, for maintaining a template of the target, and for matching the former against the latter. As pointed out above, we are not the first to show that these areas are linked to attentional control in general (4, 5, 29) or to the AB task in particular (5). However, whereas previous studies revealed these areas to be generally more active during attentionally taxing conditions, the present findings demonstrate that these areas are (*i*) mutually coactive and (*ii*) form a dynamically interacting network.

Synchronization in the Target-Related Network. To reiterate, our findings suggest that communication within the target-related network proceeds via neural synchronization at a frequency of ≈15 Hz (beta band). Before discussing the implications of these observations, let us first consider two possible objections against our findings.

First, one could erroneously assume that a modulation of the *amplitude* of neural activity such as we observe in the present study gives rise to the modulation of synchronization, which we report as our significant finding. However, in addition to the fact that the amplitude is removed before computation of phase synchronization, such amplitude has a different timing when compared with phase synchronization. Whereas the global power (mean over all sensors and subjects) shows a peak ≈400 ms after target onset (Fig. 1), phase synchronization peaks ≈260 ms after target onset. This observation demonstrates that local processing, as indicated by power changes, can be distinguished from distributed processing as indicated by changes in phase synchronization. Although power in the beta band was modulated with the presentation frequency (especially in occipital areas), creating surrogate data by randomly changing phases demonstrated that the modulation of SI cannot be explained by modulation of power.

A second possible objection could mistakenly arise from the argument that different channel groups pick up the signal from the same activated area, then appearing as synchronization. We can, however, exclude this possibility: When we correlated the sensitivity profiles[‡‡] of all channel groups, we found that the strongest correlation (obtained for frontal right and temporal right) was associated with only weak phase synchronization and the strongest synchronization (between frontal left and posterior parietal right) with a very weak profile correlation of −0.07. Thus, there is no reason to believe that our synchronization results are contaminated by overlap of sensitivity profiles of channel groups.

Having ruled out these alternative accounts, we conclude that the visual–attentional network does indeed communicate by neural phase synchronization in the beta band, in the particular experimental paradigm under consideration. In support of our finding, transient phase synchronization has been frequently suggested to mediate the integration of cortically distributed processes (6, 7, 15, 30–34). Moreover, previous studies suggest a particular role of synchronization in long-range interarea communication. Recordings from electrodes implanted in cat visual, parietal, and motor cortex showed synchronization between visual and parietal, and parietal and motor cortex neural activity that changed with behavior (35). Similarly, synchronization of neural activity occurs in a go/no-go paradigm between different areas of the cat visual system (36). In this study, time lags of oscillatory activity in the different areas suggest a top-down influence mainly in the 4- to 12-Hz frequency range. In humans, transient long-range phase synchronization was observed between different electrodes covering occipital, parietal, and frontal areas (7). Maximum synchronization in the gamma frequency band appeared ≈250 ms after visual presentation of human faces. In another study, steady-state magnetic fields were recorded during the presentation of two different

[‡‡]The sensitivity profile of a sensor contains at each point in the brain the measurement value that a unit source at this point would generate in the sensor.

gratings that were presented monocularly with different flicker frequencies (37). Depending on the percept, inter- and intrahemispheric synchronization was observed at the frequency corresponding to the flicker frequency of the observed grating.

Interestingly, in contrast to some of the mentioned studies, phase synchronization in the present experiment took place in the beta band at a frequency of ≈15 Hz. Selection of the beta band was motivated by the respective maximum difference between target and distractor trials in the time–frequency analysis, a criterion that reflects the dominance of beta-band synchronization but should not be taken to imply that other frequency bands play no role at all. The frequency of 15 Hz is close to the first harmonic of the stimulus presentation frequency (6.85 Hz), perhaps suggesting that the latter affected the former. If so, at least some differences in synchronization frequencies observed across the available studies may reflect theoretically less interesting differences in task and presentation methods.

There is convincing evidence that the beta band plays an important role in attentional processes. Phase synchronization in the beta band between extrastriate areas was observed in intracranial recordings during maintenance of objects in short-term memory (38). In addition, beta-band synchronization between temporal and parietal areas was evident in EEG recordings during object processing (39). Specifically, the beta frequency range has been linked to cognitive processes and visual attention (40, 41) and was very recently reported to exhibit perception-related modulation in awake monkeys during binocular rivalry (42). In addition, simulation studies have revealed that the beta frequency has characteristics that are favorable for long-range interactions, whereas the gamma frequency band seems to be optimal for local processing (43, 44). If so, the beta frequency band seems to be a prime candidate for mediating the interactions of a widely distributed (attentional) network.

Perhaps more importantly than determining the frequency the members of the attentional network use to communicate, the challenge is to figure out the content and functions of this synchronization. Our findings reveal two such functions. First, we observed that good performance on T2 is associated with a particularly tight coupling of the network components when processing the target. Second, we see active suppression of communication when processing nontargets, occurring directly before and after a target. Thus, an important conclusion from our findings is that neural (de)synchronization serves to dynamically adjust the network state, linking spatially disparate members of the network together. In turn, this enables equal treatment of a given stimulus event in all relevant processing subsystems, be it coherent support for a target or coherent suppression of the preceding and following nontarget. There are reasons to assume that these stimulus preferences originate in prefrontal components (1), which then may entrain other components by means of beta-band synchronization.

In summary, our study provides a dynamic view of the attentional modulation of communication between brain areas. Such a network consists of areas that are known to be involved in target detection, visual attention, and working memory (processes that are required for the successful execution of any visually based task, such as the one under consideration). The neural communication within this network reveals a striking correspondence to the actual behavioral outcome, that is, to the likelihood to detect and report a visual target. We conclude that synchronization/desynchronization appears to be a candidate mechanism for enhancing target processing while at the same time avoiding interference by suppressing the processing of nontargets (e.g., masks), respectively. Indeed such a mechanism may define an important aspect of what we commonly refer to as "attention."

We thank Mrs. E. Rädisch for technical help with the MRI scans and Sander Martens for participation in the data acquisition. This study was supported by Volkswagen Stiftung Grants I/76764 and I/73240.

1. Desimone, R. & Duncan, J. (1995) *Annu. Rev. Neurosci.* **18,** 193–222.
2. Corbetta, M. & Shulman, G. L. (2002) *Nat. Rev. Neurosci.* **3,** 201–215.
3. Nobre, A. C., Sebestyen, G. N., Gitelman, D. R., Mesulam, M. M., Frackowiak, R. S. & Frith, C. D. (1997) *Brain* **120,** 515–533.
4. Hopfinger, J. B., Buonocore, M. H. & Mangun, G. R. (2000) *Nat. Neurosci.* **3,** 284–291.
5. Marois, R., Chun, M. M. & Gore, J. C. (2000) *Neuron* **28,** 299–308.
6. Singer, W. (1999) *Neuron* **24,** 49–65, 111–125.
7. Rodriguez, E., George, N., Lachaux, J. P., Martinerie, J., Renault, B. & Varela, F. J. (1999) *Nature* **397,** 430–433.
8. Chen, Y., Seth, A. K., Gally, J. A. & Edelman, G. M. (2003) *Proc. Natl. Acad. Sci. USA* **100,** 3501–3506.
9. Steinmetz, P. N., Roy, A., Fitzgerald, P. J., Hsiao, S. S., Johnson, K. O. & Niebur, E. (2000) *Nature* **404,** 187–190.
10. Gross, J., Timmermann, L., Kujala, J., Dirks, M., Schmitz, F., Salmelin, R. & Schnitzler, A. (2002) *Proc. Natl. Acad. Sci. USA* **99,** 2299–2302.
11. Miltner, W. H., Braun, C., Arnold, M., Witte, H. & Taub, E. (1999) *Nature* **397,** 434–436.
12. Sarnthein, J., Petsche, H., Rappelsberger, P., Shaw, G. L. & von Stein, A. (1998) *Proc. Natl. Acad. Sci. USA* **95,** 7092–7096.
13. Classen, J., Gerloff, C., Honda, M. & Hallett, M. (1998) *J. Neurophysiol.* **79,** 1567–1573.
14. Mima, T., Oluwatimilehin, T., Hiraoka, T. & Hallett, M. (2001) *J. Neurosci.* **21,** 3942–3948.
15. Varela, F., Lachaux, J. P., Rodriguez, E. & Martinerie, J. (2001) *Nat. Rev. Neurosci.* **2,** 229–239.
16. Raymond, J. E., Shapiro, K. L. & Arnell, K. M. (1992) *J. Exp. Psychol. Hum. Percept. Perform.* **18,** 849–860.
17. Duncan, J., Ward, R. & Shapiro, K. (1994) *Nature* **369,** 313–315.
18. Shapiro, K. L., Raymond, J. E. & Arnell, K. M. (1994) *J. Exp. Psychol. Hum. Percept. Perform.* **20,** 357–371.
19. Luck, S., Vogel, E. & Shapiro, K. (1996) *Nature* **383,** 616–618.
20. Brehaut, J. C., Enns, J. T. & Di Lollo, V. (1999) *Percept. Psychophys.* **61,** 1436–1448.
21. Giesbrecht, B. & Di Lollo, V. (1998) *J. Exp. Psychol. Hum. Percept. Perform.* **24,** 1454–1466.
22. Ahonen, A. I., Hämäläinen, M. S., Kajola, M. J., Knuutila, J. E. T., Laine, P. P., Lounasmaa, O. V., Parkkonen, L. T., Simola, J. T. & Tesche, C. D. (1993) *Physica Scripta* **T49,** 198–205.
23. Gross, J., Kujala, J., Hamalainen, M., Timmermann, L., Schnitzler, A. & Salmelin, R. (2001) *Proc. Natl. Acad. Sci. USA* **98,** 694–699.
24. Enns, J. T. & Lollo, V. D. (1997) *Psychol. Sci.* **8,** 135–139.
25. Luck, S. J., Chelazzi, L., Hillyard, S. A. & Desimone, R. (1997) *J. Neurophysiol.* **77,** 24–42.
26. McCarthy, G., Puce, A., Constable, R. T., Krystal, J. H., Gore, J. C. & Goldman-Rakic, P. (1996) *Cereb. Cortex* **6,** 600–611.
27. Quintana, J. & Fuster, J. M. (1999) *Cereb. Cortex* **9,** 213–221.
28. Fletcher, P. C. & Henson, R. N. (2001) *Brain* **124,** 849–881.
29. Friedman-Hill, S. R., Robertson, L. C., Desimone, R. & Ungerleider, L. G. (2003) *Proc. Natl. Acad. Sci. USA* **100,** 4263–4268.
30. von der Malsburg, C. (1999) *Neuron* **24,** 95–104, 111–125.
31. Singer, W. (1999) *Nature* **397,** 391, 393.
32. Singer, W. (1999) *Curr. Opin. Neurobiol.* **9,** 189–194.
33. Fries, P., Roelfsema, P. R., Engel, A. K., Konig, P. & Singer, W. (1997) *Proc. Natl. Acad. Sci. USA* **94,** 12699–12704.
34. Engel, A. K., Fries, P. & Singer, W. (2001) *Nat. Rev. Neurosci.* **2,** 704–716.
35. Roelfsema, P. R., Engel, A. K., Konig, P. & Singer, W. (1997) *Nature* **385,** 157–161.
36. von Stein, A., Chiang, C. & Konig, P. (2000) *Proc. Natl. Acad. Sci. USA* **97,** 14748–14753.
37. Srinivasan, R., Russell, D. P., Edelman, G. M. & Tononi, G. (1999) *J. Neurosci.* **19,** 5435–5448.
38. Tallon-Baudry, C., Bertrand, O. & Fischer, C. (2001) *J. Neurosci.* **21,** RC177.
39. von Stein, A., Rappelsberger, P., Sarnthein, J. & Petsche, H. (1999) *Cereb. Cortex* **9,** 137–150.
40. Liang, H., Bressler, S. L., Ding, M., Truccolo, W. A. & Nakamura, R. (2002) *NeuroReport* **13,** 2011–2015.
41. Wrobel, A. (2000) *Acta Neurobiol. Exp.* **60,** 247–260.
42. Gail, A., Brinksmeyer, H. & Eckhorn, R. (2004) *Cereb. Cortex* **14,** 300–313.
43. Kopell, N., Ermentrout, G. B., Whittington, M. A. & Traub, R. D. (2000) *Proc. Natl. Acad. Sci. USA* **97,** 1867–1872.
44. Bibbig, A., Traub, R. D. & Whittington, M. A. (2002) *J. Neurophysiol.* **88,** 1634–1654.